

## Realistic Full Wave Modeling of Focal Plane Array Pixels

Salvatore Campione<sup>1</sup>, Larry K. Warne<sup>1</sup>, Roy E. Jorgenson<sup>1</sup>, Paul S. Davids<sup>2</sup>,  
and David W. Peters<sup>2</sup>

<sup>1</sup>Electromagnetic Theory Department  
Sandia National Laboratories, Albuquerque, NM 87185, USA  
sncampi@sandia.gov, lkwarne@sandia.gov, rejorge@sandia.gov

<sup>2</sup>Applied Photonic Microsystems Department  
Sandia National Laboratories, Albuquerque, NM 87185, USA  
pdavids@sandia.gov, dwpeter@sandia.gov

**Abstract** — In this paper we investigate full-wave simulations of realistic implementations of multifunctional nanoantenna enabled detectors (NEDs). We focus on a 2x2 pixelated array structure that supports two wavelengths of operation. We design each resonating structure independently using full-wave simulations with periodic boundary conditions mimicking the whole infinite array. We then construct a supercell made of a 2x2 pixelated array with periodic boundary conditions mimicking the full NED; in this case, however, each pixel comprises 10-20 antennas per side. In this way, the cross-talk between contiguous pixels is accounted for in our simulations. We observe that, even though there are finite extent effects, the pixels work as designed, each responding at the respective wavelength of operation. This allows us to stress that realistic simulations of multifunctional NEDs need to be performed to verify the design functionality by taking into account finite extent and cross-talk effects.

**Index Terms** — Cross-talk, finite extent, multifunctional detectors, nanoantenna enabled detectors.

### I. INTRODUCTION

Infrared detector arrays based on narrow bandgap, III-V semiconductors have made tremendous progress in the last decade [1]. Within III-V semiconductor alloys, those containing antimony have enabled certain heterostructures to exhibit a broken gap that is advantageous in some newer detector designs [2, 3]. These narrow bandgap semiconductors also show promise in electronic applications such as high-frequency, low-noise high-electron-mobility-transistors [4]. Highly doped semiconductor materials acting as plasmonic materials have also been explored [5-7].

In recent years, infrared detection has been enhanced through the use of plasmonic nanoantenna arrays on top of semiconductor heterostructures that

contain the active material of a photodetector [8-12] (see schematic in Fig. 1 (a)). We define these detectors as *nanoantenna enabled detectors* (NEDs). The nanoantenna arrays generate enhanced fields that induce enhanced absorption within the active material of a photodetector, enhancing its overall performance. The standard way to design such a nanoantenna array is by using full-wave simulations employing periodic boundary conditions: this kind of simulation mimics an infinitely extended array.

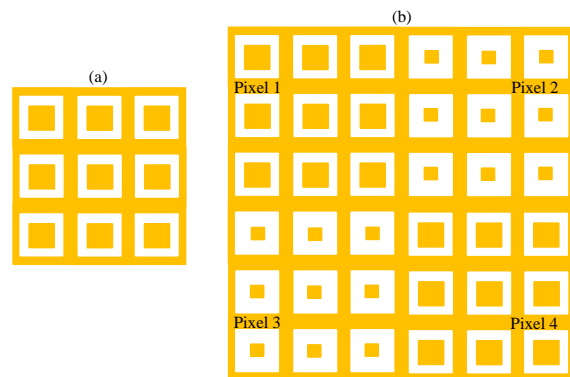


Fig. 1. (a) Illustration of a gold nanoantenna array. (b) Illustration of a multifunctional nanoantenna enabled detector made of a 2x2 pixel array, where each pixel may perform a different functionality.

In general, there is the need to have multifunctional detectors, and this can be potentially realized using NEDs. Two alternative options exist: (1) one NED that can change its performance via external stimuli, such as a bias voltage; and (2) multiple NEDs interleaved in space (see schematic in Fig. 1 (b), also referred to as pixelated arrays), where each pixel is designed to perform different functionalities. While the former is a very attractive platform, the difficulties that are inherent

to such a tunable design make the use of pixelated arrays the most viable solution for multifunctional NEDs. Functionalities may include different polarization properties, different spectral properties, etc. In this paper, we focus on modeling dual-band NEDs made of pixelated arrays. While each resonating structure can be independently designed using full-wave simulations with periodic boundary conditions, there is no guarantee that a pixelated array would perform as desired. This is because, (1) the extent of each pixel is finite, and thus comprises of a finite number of unit cells and may not fulfill the infinite condition imposed by the periodic boundary conditions; and (2) the cross-talk between contiguous pixels may dramatically affect the NED performance. We then construct a supercell made of a  $2 \times 2$  pixelated array with periodic boundary conditions that allows us to take into account both the finite extent of each pixel as well as their cross-talk. We observe that the pixels work as designed, each responding at the respective wavelength of operation with some smaller interactions between pixels. However, this allows us to stress that realistic simulations of multifunctional NEDs need to be performed to verify the design functionality and improve their performance.

## II. DESIGN OF THE NANOANTENNA STRUCTURES AT THE TWO WAVELENGTHS OF OPERATION

We aim to design a multifunctional NED structure that contains subpixels that work at different wavelengths. For simplicity of discussion, we focus on 4 pixels, displaced in a  $2 \times 2$  pixelated array in a checker pattern as in Fig. 1 (b), where each diagonal pair works at two different wavelengths: 1)  $\sim 10 \mu\text{m}$  with  $\sim 1.5 \mu\text{m}$  bandwidth; and 2)  $\sim 8 \mu\text{m}$  with  $\sim 1 \mu\text{m}$  bandwidth. Each pixel is based on a gold nanoantenna design as in Fig. 1 (a) on top of a semiconductor heterostructure as illustrated in Fig. 2 (a). The complex index of refraction  $n_c = n + ik$  of the absorber layer is reported versus wavelength in Fig. 2 (b). The monochromatic time harmonic convention,  $\exp(-i\omega t)$ , is used here and throughout the paper, and is suppressed hereafter. We employ finite difference time domain (FDTD) simulations using the commercial software FDTD Lumerical. The commercial software accepts the dispersive properties in Fig. 2 (b) and creates a multi-coefficient material model for use in the FDTD simulation.

We first design the two nanoantenna designs separately using full-wave simulations employing periodic boundary conditions. We have explored various mesh discretizations as to achieve a converged, accurate result. The design working at  $\sim 10 \mu\text{m}$  is shown in Fig. 3. The total absorption spectrum versus wavelength under normal plane wave incidence is reported as a black line in Fig. 3: high absorption is observed at  $\sim 9.75 \mu\text{m}$  and

also at  $\sim 6.7 \mu\text{m}$ . The important aspect of this design is that it exhibits a minimum in absorption at  $\sim 8 \mu\text{m}$  to minimally interfere with the second band of interest (ideally this minimum should be zero). We plot in the same figure as red dashed curve the absorption in the absorber layer: one can note that this is a lower amount of energy than the black curve, indicating that the remaining energy is dissipated by the nanoantennas and the back mirror. We report electric field magnitude plots (in a  $x$ - $y$  plane cut within the absorber layer) as insets of Fig. 3 at the wavelengths indicated by the vertical cyan lines, and one can see enhanced fields at the two resonances.

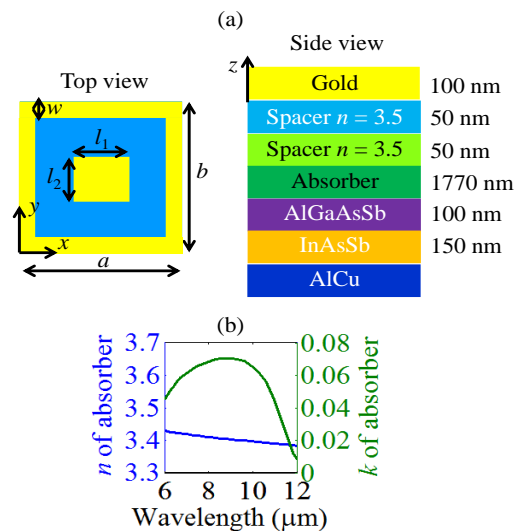


Fig. 2. (a) Top view and side view of a unit cell of the nanoantenna array on top of the semiconductor heterostructure: periods  $a$  and  $b$ , patch sides  $l_1$  and  $l_2$ , and width  $w$ . (b) Real part  $n$  and imaginary part  $k$  of the complex index of refraction of the absorber versus wavelength.

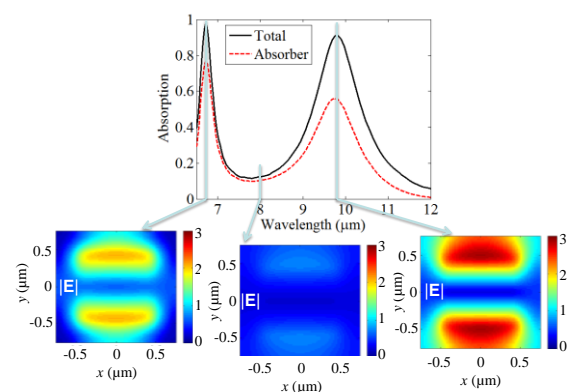


Fig. 3. Absorption spectrum of the nanoantenna design working at  $\sim 10 \mu\text{m}$  with  $a = b = 1500 \text{ nm}$ ,  $l_1 = l_2 = 900 \text{ nm}$  and  $w = 50 \text{ nm}$ . The insets show maps of the magnitude of the electric field at  $\sim 6.7 \mu\text{m}$ ,  $\sim 8 \mu\text{m}$ , and  $\sim 9.75 \mu\text{m}$ .

The design working at  $\sim 8 \mu\text{m}$  is shown in Fig. 4, where we report the total absorption spectrum versus wavelength under normal plane wave incidence as a black line: high absorption is observed at  $\sim 8 \mu\text{m}$ . The important aspect of this design is that it exhibits a minimum in absorption at  $\sim 10 \mu\text{m}$  to minimally interfere with the second band of interest. We plot in the same figure as red dashed curve the absorption in the absorber layer: one can note that this is a lower amount of energy than indicated by the black curve, indicating that the remaining energy is dissipated by the nanoantennas and the back mirror. We report electric field magnitude plots (in a  $x$ - $y$  plane cut within the absorber layer) at the wavelengths indicated by the vertical cyan lines, and one can see enhanced fields at the resonance supported by this structure.

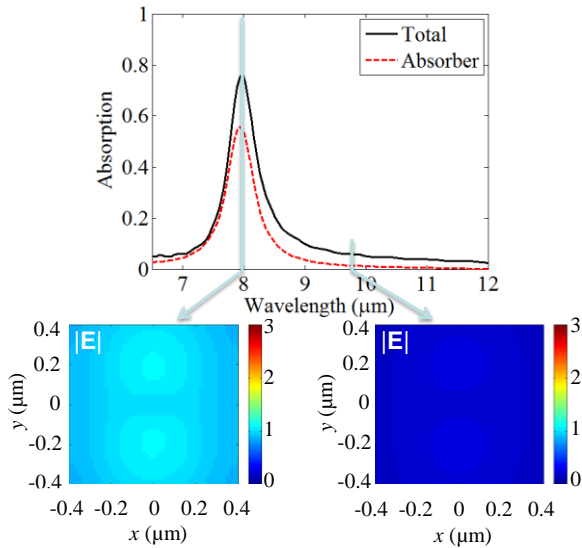


Fig. 4. Absorption spectrum of the nanoantenna design working at  $\sim 8 \mu\text{m}$  with  $a = b = 800 \text{ nm}$ ,  $l_1 = l_2 = 150 \text{ nm}$  and  $w = 50 \text{ nm}$ . The insets show maps of the magnitude of the electric field at  $\sim 8 \mu\text{m}$  and  $\sim 9.75 \mu\text{m}$ .

### III. REALISTIC DUAL-BAND NANOANTENNA ENABLED DETECTORS

We construct a  $30 \mu\text{m} \times 30 \mu\text{m}$  NED supercell made of a  $2 \times 2$  pixelated array as shown in Fig. 5, where each  $15 \mu\text{m} \times 15 \mu\text{m}$  pixel in the main diagonal is a finite extent version of the design reported in Fig. 4 and each  $15 \mu\text{m} \times 15 \mu\text{m}$  pixel in the anti-diagonal is a finite extent version of the design reported in Fig. 3: because of the different periods of the two designs, the main diagonal pixels contain  $10 \text{ unit cells} \times 10 \text{ unit cells}$ , whereas the anti-diagonal pixels contain  $18 \text{ unit cells} \times 18 \text{ unit cells}$ . Because of the finite extent of each pixel, it is of interest to determine if the detector will behave as designed, or rather the optical properties would be affected by cross-talk between the different pixels.

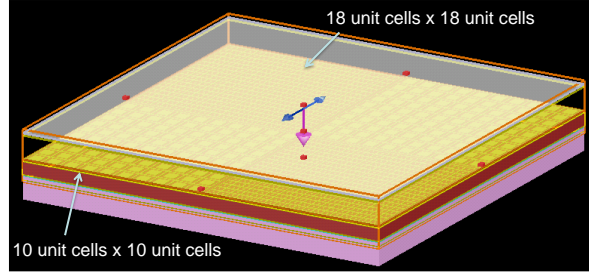


Fig. 5. Illustration of the  $2 \times 2$  pixelated array NED in checker pattern. Note the finite extent of each pixel.

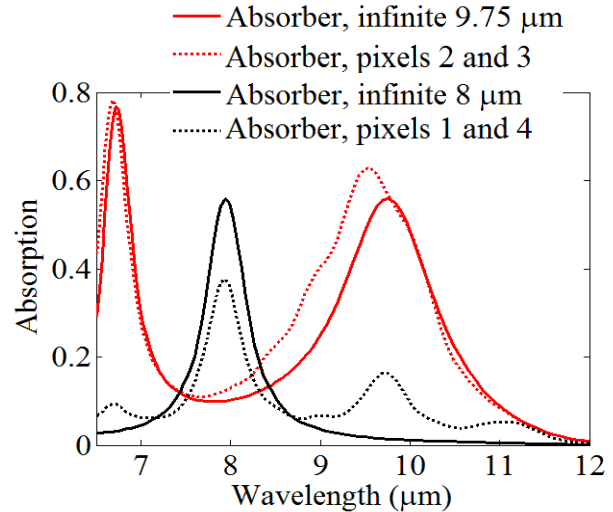


Fig. 6. Absorption spectrum of the dual-band detector in Fig. 5, highlighting the contributions of main-diagonal and anti-diagonal pixels separately (dotted lines). The results are compared to the infinite arrays (solid lines).

The simulated structure is  $5\lambda \times 5\lambda$  at  $\lambda = 6 \mu\text{m}$ . In order to accurately model the pixelated array, we made use of a supercomputer and used a mesh similar to the one employed in the periodic simulations. We first plot in Fig. 6 the absorption spectrum of the dual-band detector in Fig. 5, restricting the contributions to the main-diagonal (Pixels 1 and 4) and anti-diagonal pixels (Pixels 2 and 3) separately (as indicated in Fig. 1 (b)). One can see that the pixel supporting the resonance at  $\sim 10 \mu\text{m}$  behaves better than designed, given that the absorber receives more power (see solid versus dotted red curves). Some minor finite extent and cross-talk effects are observed as a shoulder at  $\sim 9 \mu\text{m}$ . When looking at the result relative to the pixel supporting the resonance at  $\sim 8 \mu\text{m}$ , we see that it behaves worse than designed. In particular, we see that the absorber receives less power, and absorbs in frequency bands where it shouldn't, due to evident finite extent and cross-talk effects. Nonetheless, the overall behavior of the NED array is satisfactory, and these realistic simulations

can be used to assess (and possibly improve) NED performance.

The complete NED supercell detector design operation is summarized in Fig. 7, where we report the total absorption spectrum versus wavelength under normal plane wave incidence as a black line: high absorption is observed at  $\sim 9.75 \mu\text{m}$ ,  $\sim 8 \mu\text{m}$ , and  $\sim 6.7 \mu\text{m}$  --- the three resonances observed in Sec. 2 for the individual designs. We plot in the same figure as red dashed curve the absorption in the absorber layer: one can note that this is a lower amount of energy than the black curve, indicating that the remaining energy is dissipated by the nanoantennas and the back mirror. We report electric field magnitude plots in the insets of Fig. 7 (in a  $x$ - $y$  plane cut within the absorber layer) at the wavelengths indicated by the vertical cyan lines, and one can see enhanced fields at the resonances, with the anti-diagonal pixels mainly illuminated at  $\sim 9.75 \mu\text{m}$ , and the main-diagonal pixels mainly illuminated at  $\sim 8 \mu\text{m}$ . This shows that, although some cross-talk is inevitably present, the dual-band detector can actually work effectively as designed. Because these are uniformly illuminated arrays, it seems reasonable that the cross-talk effects observed in Fig. 7 are likely due to just off-resonance response of the pixels to the uniform illumination.

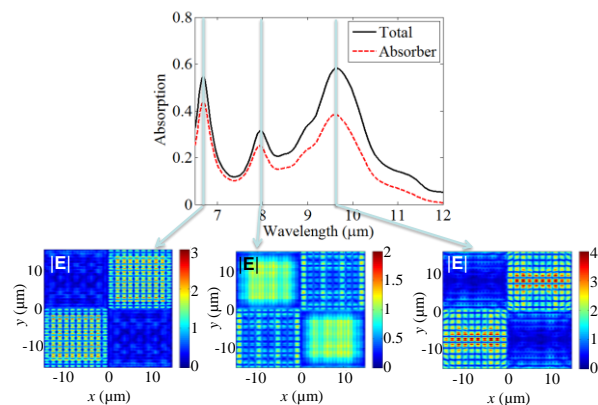


Fig. 7. Absorption spectrum of the dual-band NED in Fig. 5. The insets show maps of the magnitude of the electric field at  $\sim 6.7 \mu\text{m}$ ,  $\sim 8 \mu\text{m}$ , and  $\sim 9.75 \mu\text{m}$ .

#### IV. CONCLUSION

In this paper we have investigated full-wave simulations of realistic implementations of multifunctional nanoantenna enabled detectors. We have shown that it is pivotal to simulate the entire structure comprising finite extent pixels to correctly account for the cross-talk between contiguous pixels. We observed that, even though there are finite extent and cross-talk effects affecting the performance of the dual-band NED, the pixels work as designed, each responding at the respective

wavelength of operation. Nonetheless, realistic simulations of multifunctional detectors need to be performed to verify the design functionality by taking into account finite extent and cross-talk effects. Although we have analyzed normal incidence illumination of our NED detector structure, the envisioned applications will be subjected to up to 10 degrees oblique incidence illumination. We have modeled both transverse electric (TE) and magnetic (TM) oblique incidence (10 degrees) and observed very minimal change to the normal incidence case.

#### ACKNOWLEDGMENT

This work was supported by the Laboratory Directed Research and Development program at Sandia National Laboratories. Sandia National Laboratories is a multimission laboratory managed and operated by National Technology and Engineering Solutions of Sandia, LLC.; a wholly owned subsidiary of Honeywell International, Inc., for the U.S. Department of Energy's National Nuclear Security Administration under contract DE-NA-0003525.

#### REFERENCES

- [1] N. K. Dhar, R. Dat, and A. K. Sood, "Advances in infrared detector array technology," in *Optoelectronics - Advanced Materials and Devices*, S. L. Pyshkin and J. M. Ballato, Eds., InTech, 2013.
- [2] P. Martyniuk, M. Kopytko, and A. Rogalski, "Barrier infrared detectors," *Opto-Electronics Review*, vol. 22, pp. 127-146, 2014.
- [3] E. A. Plis, "InAs/GaSb type-II superlattice detectors," *Advances in Electronics*, vol. 2014, p. 12, 2014.
- [4] C. Liu, Y. Li, and Y. Zeng, "Progress in antimonide based III-V compound semiconductors and devices," *Engineering*, vol. 2, pp. 617-624, 2010.
- [5] S. Law, R. Liu, and D. Wasserman, "Doped semiconductors with band-edge plasma frequencies," *Journal of Vacuum Science & Technology B*, vol. 32, p. 052601, 2014.
- [6] D. Wei, C. Harris, C. C. Bomberger, J. Zhang, J. Zide, and S. Law, "Single-material semiconductor hyperbolic metamaterials," *Optics Express*, vol. 24, pp. 8735-8745, 2016/04/18 2016.
- [7] S. Law, D. C. Adams, A. M. Taylor, and D. Wasserman, "Mid-infrared designer metals," *Optics Express*, vol. 20, pp. 12155-12165, 2012/05/21 2012.
- [8] D. W. Peters, C. M. Reinke, P. S. Davids, J. F. Klem, D. Leonhardt, J. R. Wendt, *et al.*, "Nanoantenna-enabled midwave infrared focal plane arrays," pp. 83533B-83533B-6.
- [9] S. Choi and K. Sarabandi, "Bowtie nanoantenna integrated with indium gallium arsenide antimonide for uncooled infrared detector with enhanced sensitivity," *Applied Optics*, vol. 52, pp. 8432-8438,

2013/12/10 2013.

- [10] D. W. Peters, P. S. Davids, J. K. Kim, D. Leonhardt, T. E. Beechem, S. W. Howell, *et al.*, "Application of plasmonic subwavelength structuring to enhance infrared detection," pp. 899419-899419-6, 2014.
- [11] M. D. Goldflam, E. A. Kadlec, B. V. Olson, J. F. Klem, S. D. Hawkins, S. Parameswaran, *et al.*, "Enhanced infrared detectors using resonant structures combined with thin type-II superlattice absorbers," *Applied Physics Letters*, vol. 109, p. 251103, 2016/12/19 2016.
- [12] M. D. Goldflam, S. D. Hawkins, S. Parameswaran, A. Tauke-Pedretti, L. K. Warne, D. W. Peters, *et al.*, "Next-generation infrared focal plane arrays for high-responsivity low-noise applications," in *2017 IEEE Aerospace Conference*, pp. 1-7, 2017.



**Salvatore Campione** received a Laurea triennale degree (cum laude) and a Laurea Magistrale degree (cum laude) in Electronic Engineering from the Polytechnic of Turin, Italy, in 2007 and 2009, respectively. He also received a Master of Science degree in

electrical and computer engineering from the University of Illinois at Chicago, IL, USA, in 2009, and a Doctor of Philosophy degree in electrical and computer engineering from the University of California Irvine, CA, USA, in 2013.

Dr. Campione has been a visiting scholar at the U.S. Army Charles M. Bowden Research Center, RDECOM, Redstone Arsenal, Huntsville, AL, USA in 2012 and at the Center for Integrated Nanotechnologies at Sandia National Laboratories, Albuquerque, NM, USA in 2012 and 2013. He joined Sandia National Laboratories, Albuquerque, NM, USA as a Postdoctoral Appointee in 2014, and became a Senior Member of Technical Staff in 2016. He has published more than 65 peer-reviewed journal articles, more than 100 conference papers, 1 issued patent, and 2 book chapters. His research interests include electromagnetic theory, antennas, metamaterials and their applications, plasmonics in nanostructures, and optical devices for energy and optoelectronic applications.

Dr. Campione is a member of ACES, SPIE, IEEE, the IEEE Photonics Society, the IEEE Antennas and Propagation Society, and the IEEE Eta Kappa Nu (IEEE-HKN) Society. Among other awards, he received a 2013 Marconi Society Paul Baran Young Scholar Award, the 2016 IEEE-HKN Outstanding Young Professional Award, and the 2017 ACES Early Career Award.



**Larry K. Warne** received the B.S.E.E. degree from Fairleigh Dickinson University, Teaneck, NJ, in 1976 and the M.S.E.E. and Ph.D. degrees from the California Institute of Technology, Pasadena, in 1977 and 1984, respectively.

Since 1978, he has been employed at Sandia National Laboratories, Albuquerque, NM, where he is currently a Distinguished Member of the Technical Staff.



**Roy E. Jorgenson** was born in Portland, OR, on May 11, 1955. He received the B.S.E.E. degree from the University of Colorado, Boulder, in 1977 and the M.S. and Ph.D. degrees in electrical engineering from the University of Illinois at Urbana-Champaign, in 1985 and 1989, respectively.

He served as an Officer in the U.S. Army at Field Station Berlin, Berlin, Germany, until 1983. Since 1989, he has been with Sandia National Laboratories, Albuquerque, NM.



**Paul S. Davids** received his Ph.D in theoretical condensed matter physics in 1993 from Indiana University while as a graduate research associate in Theoretical Division at Los Alamos National Lab. He was then a postdoc in the Electronics Device and Materials

group from 1993-1996. He then joined Intel Oregon and held various research positions from 1996-2008. He joined Sandia National lab in 2008 where he is currently a PMTS. He has over 75 papers and 23 issued patents with 18 pending.



**David W. Peters** received the B.S., M.S., and Ph.D. degrees in electrical engineering from the Georgia Institute of Technology, Atlanta, in 1992, 1993, and 2001, respectively. His graduate research was in the area of numerical modeling of diffractive optic structures. He is currently with Sandia National Laboratories, Albuquerque, NM, working on modeling of diffractive optics and photonic bandgap structures.

Dr. Peters is a Member of the Optical Society of America.